Table 1 Numerical test conditions and the ratios of predicted flow rates

Flow case	$\frac{v_w}{U_0}$	ψ_{lower}[a]	ψ_{upper}[b]	$\frac{Q_{\text{inj\_rez}/2}}{Q_{\text{in}}}$[c]	$\frac{\psi_{\text{lower}}}{\psi_{\text{upper}}}$[d]	$\frac{Q_{r\_\max}}{Q_{\text{in}}}$[e]	$\frac{\Delta Q}{Q_{\text{inj\_rez}/2}}$[f]
A	0	2.50%	16.0%	0	15.63%	2.99%	——
B	1.47%	0.75%	6.0%	1.43%	12.50%	1.83%	75.55%
C	2.05%	0.45%	6.0%	1.89%	7.50%	0.84%	20.61%
D	7.87%	——	——	4.90%	——	——	——

[a] Stream function at the lower boundary of the new shear layer.
[b] Stream function at the upper boundary of the new shear layer.
[c] $Q_{\text{inj\_rez}/2}$-half-injection rate within the region of 4.45 times of step height.
[d] Percentage of the new shear layer deflected upstream the reattachment point.
[e] $Q_{r\_\max}$-maximal reverse flow rate.
[f] $\Delta Q = Q_{r\_\max} - \psi_{\text{lower}} Q_{\text{in}}$.

located at $0.5x_r$, the present choice of $\Delta Q/Q_{\text{inj\_rez}/2}$ conveniently gives the wall injection that most probably contributes to the maximal strength of reversal flow. For case A, without mass injection, the entrainment is less than 2.5% of the total inflow rate, which is very close to the maximal reverse flow rate in the recirculating zone. For cases B and C the more the mass is injected from the wall, the less the entrainment and maximal reverse flow rate becomes. This trend is clearly related to both the enlargement of the corner eddy and the lift of the main recirculating bubble from the porous wall. About 75.55% of the injected mass can contribute to the maximal reverse flow in case B, whereas only 20.61% in case C. All of these phenomena are beneficial to the analysis of the ignition in SFRJ-based systems or transpiration cooling in separated flows.

Conclusions

This study investigates numerically the effects of lateral injection rate on the inlet mainstream that deflects the reattachment point upstream with special focus on the intimately relation between the maximal reverse rate and the entrainment fluid. The analysis reveals that the enhancement of blowing rate suppresses apparently the strongest reversal strength because of the enlargement of the corner eddy and the lift of the main recirculating bubble from the porous wall. For the case without wall injection, about 15.63% of the new shear layer is deflected upstream the reattachment point, whereas approximately 12.5 and 7.5% of the new shear layer are deflected upstream for the flow fields B and C, respectively.

References

[1] Yang, J. T., Tsai, B. B., and Tsai, G. L., "Separated-Reattaching Flow over a Backstep with Uniform Normal Mass Bleed," *Journal of Fluids Engineering*, Vol. 116, No. 1, 1994, pp. 29–35.

[2] Richardson, J., de Groot, W. A., Jadoga, J. I., Walterick, R. E., Hubbartt, J. E., and Strahle, W. C., "Solid Fuel Ramjet Simulator Results: Experiment and Analysis in Cold Flow," *Journal of Propulsion and Power*, Vol. 1, No. 6, 1985, pp. 488–493.

[3] Ma, W. J., "Transpiration Cooling Phenomena in Separated Flow Field," Ph.D. Dissertation, Dept. of Power Mechanical Engineering, National Tsing Hua Univ., Taiwan, June 2000.

[4] Pitz, R. W., and Daily, W., "Combustion in a Turbulent Mixing Layer Formed at a Rearward-Facing Step," *AIAA Journal*, Vol. 21, No. 11, 1983, pp. 1565–1570.

[5] Leonard, B. P., "A Stable Accurate Convective Modelling Procedure Based on Quadratic Upstream Interpolation," *Computers Method in Applied Mechanics and Engineering*, Vol. 19, No. 1, 1979, pp. 59–98.

[6] Patankar, S. V., *Numerical Heat Transfer and Fluid Flow*, Hemisphere, Washington, DC, 1980, pp. 79–138.

[7] Lee, S. C., "Structural and Mixing Characteristics of a Backstep Flow with Lateral Mass Injection Using LES with Near-Wall Treatment," Ph.D. Dissertation, Dept. of Power Mechanical Engineering, National Tsing Hua Univ., Taiwan, Nov. 2002.

[8] Etheridge, D. W., and Kemp, P. H., "Measurements of Turbulent Flow Downstream of a Rearward-Facing Step," *Journal of Fluid Mechanics*, Vol. 86, No. 3, 1978, pp. 545–566.

Leading-Edge Shape and Aeroengine Fan Blade Performance

A. I. Sayma* and M. Kim†
Imperial College,
London, England SW7 2BX, United Kingdom
and
N. H. S. Smith‡
Rolls–Royce plc.,
Derby, England DE24 8BJ, United Kingdom

Introduction

DURING ascent and descent, an aircraft often passes through clouds consisting of water and dirt particles, which impinge on, and erode, the leading edge of fan blades. Overall, the level of erosion increases with blade radius as the relative inlet Mach number increases. The tip region of the fan blades experiences less erosion because the nacelle offers some protection. Theoretical analysis of a bluff profile shows that locally increased accelerations around the leading edge relative to a semicircular profile result in increased shock and profile loss. In practice, this loss of efficiency due to erosion can be recouped through systematic redressing of the fan blades during scheduled servicing and overhaul.

To predict the effects of leading-edge shape on performance, the numerical prediction tools must capture the complexity of the flow near the leading edge, where high-velocity gradients and boundary-layer flow transition are observed. Some methods are now being tested for performance evaluations of more realistic geometry definitions as found during extended service operation, for example, a blunt-nosed aerofoil shape, or for performance changes resulting from surface coatings/roughness, as reported by Suder et al.[1] However, with the absence of reliable and standard transition prediction tools, the problem is a formidable challenge, and this explains why researchers have generally refrained from attempting such predictions.

This Technical Note concentrates on two aspects of the preceding discussion. First, it will be shown that overall performance and stability margin changes can be captured, without excessively fine grids or transition models, for small geometric leading-edge differences. Second, an attempt will be made to explain the underlying physical mechanisms that cause flutter margin changes.

Overview of the Numerical Methodology

The results are obtained with a well-established unsteady aeroelasticity code whose aerodynamic part is an edge-based upwind solver.[2] The time stepping is implicit; hence, large Courant–Friedrichs–Lewy numbers can be used without creating numerical instabilities. Time accuracy is ensured by a dual-time stepping technique. The code solves the Reynolds averaged Navier–Stokes equations with Baldwin–Barth, Spalart–Allmaras one-equation, or q–ζ two-equation turbulence models. The flow geometry is described using a mixture of tetrahedra, hexahedra, and wedge elements. The structural part uses a modal model obtained from a three-dimensional finite element representation.[3] The structural

Received 28 May 2002; revision received 9 December 2002; accepted for publication 30 January 2003.

*Rolls–Royce Research Fellow, Mechanical Engineering. Member of the Royal Aeronautical Society.
†Research Assistant, Centre of Vibration Engineering, Mechanical Engineering Department.
‡Staff Technologist, Fan Systems.

mode shapes are interpolated onto the fluid mesh for improved computational efficiency. During the aeroelasticity computations, the structural and fluid boundary conditions, that is, displacements and unsteady pressures, are exchanged at every time step. Consequently, the mesh is moved to a new position so that it can represent the instantaneous shape of the structure undergoing a deformation under the fluid forces. For aeroelasticity problems, such as flutter and forced response, the structural response is evaluated from the actual time history predicted at the blade surface.

For turbomachinery blades, a novel semi-unstructured meshing technique is used. This produces computationally efficient meshes compared to either fully structured or fully unstructured grids.[4] The resulting aeroelasticity system has been validated over a wide range of flutter and forced response cases[5–7] and proved to be a robust and reliable numerical tool.

Case Study

The case study examined a typical modern civil fan design operating at part speed. The computational grid for the nominal blade contains about 150,000 points, as shown in Figs. 1a and 1b. The

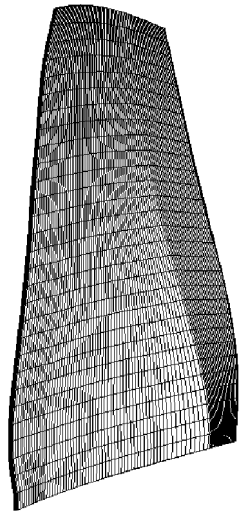

Fig. 1a Blade mesh side view.

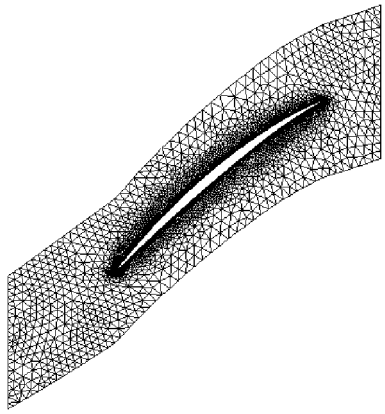

Fig. 1b Blade mesh at 85% span.

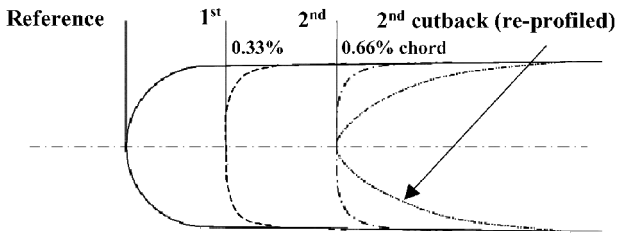

Fig. 1c LE profiles.

importance of the leading-edge (LE) shape on flutter margin were numerically assessed by constructing three other grids to represent different LE modifications. The different LE profiles are shown in Fig. 1c. These were 0.33 and 0.66% chordal cutbacks and a re-profiling of the second cutback. To simplify the modeling and grid generation, the cutback was applied along the entire span of the blade.

Steady-state solutions were obtained at a constant fan speed using imposed boundary conditions in the form of freestream total pressure, total temperature, and zero inlet swirl angle, together with a static pressure at the outflow. For all cases, a fan characteristic was mapped out by increasing the back pressure to a point close to the stall boundary (Fig. 2a). Because it is difficult to obtain steady-state solutions near stall, the static pressure profiles used were not the same for each geometry. Nevertheless, three points on the characteristic are thought to be sufficient to compute the flutter margin. It is acknowledged that the true stall boundary can only be modeled using full assembly time-accurate computations to capture the onset of rotating stall or surge. However, the present steady-state computations are believed to be sufficiently close to the stall boundary.

Flutter computations were performed for the first flap/two nodal diameter mode using cyclic symmetry, the so-called single passage analysis, with the unsteady solution being started from each steady point. In this type of analysis, shadow points are used on both sides of the periodic boundary to store the time history of the flow for a complete vibration cycle.[8] The correct interblade phase angle at the periodic boundary is then obtained by imposing a phase-lagged boundary condition from the stored quantities. The blade is vibrated periodically at a small amplitude, and the work done for the given mode is integrated over the vibration cycle. The converged value of the work done is then used to compute the logarithmic-decrement

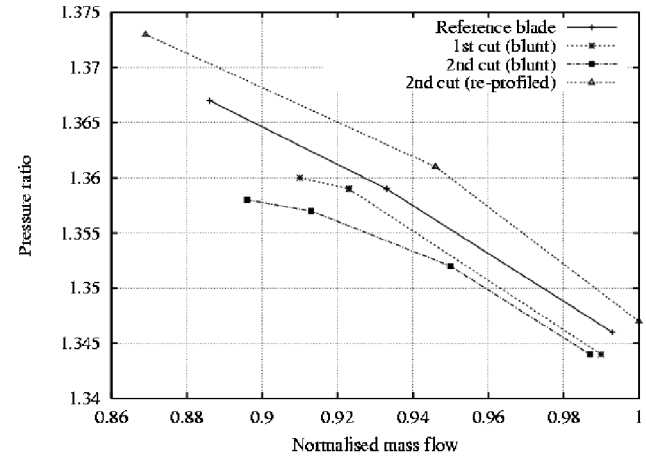

Fig. 2a Fan characteristics of different LE profiles.

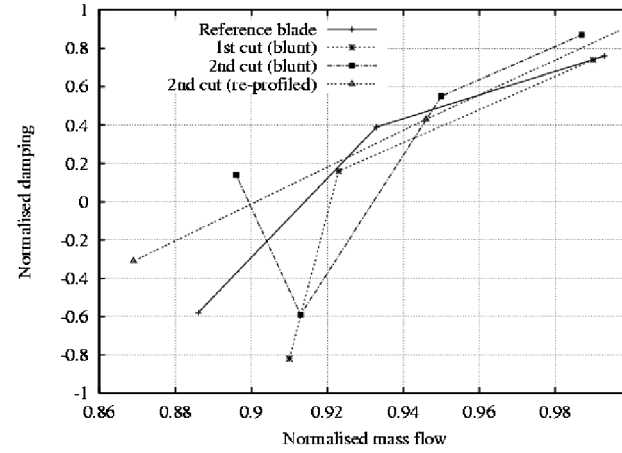

Fig. 2b Summary of log-dec values for all cases.

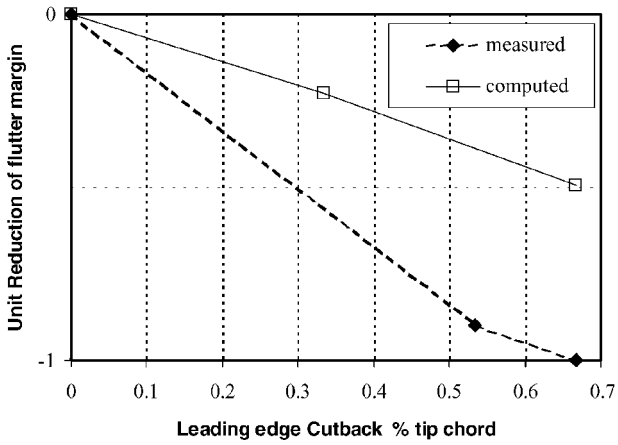

Fig. 3 Unit reduction flutter margin comparison.

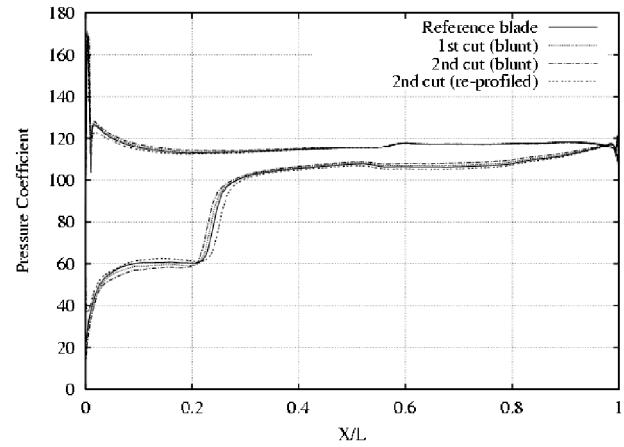

Fig. 4a Lift distributions at 85% span of all blades.

(LOG-DEC) for the given fan characteristic point; the log-dec is a measure of the flutter stability or aerodynamic damping.

The log-dec curves, shown in Fig. 2b, shows the flutter stability deteriorates as the blade operates closer to the stall boundary. The improvement in the flutter stability for the last point of the 0.66% cutback case close to the flutter boundary is thought to be artificial, which could result from the overprediction of the stall boundary using the single passage analysis. In general, the flutter stability is reduced with the increase in bluffness of the LE shape. Comparison between the predicted and measured flutter boundary variations shows good qualitative agreement; Fig. 3 shows a nominal unit change in flutter margin. A complete quantitative agreement is not expected due to the assumptions in the calculations, such as the uniform erosion along the span. Furthermore, it is noticed that the reprofiled blade showed better flutter stability over the nominal blade. This is in line with expectation and highlights stronger sensitivity to profile shape than to chordal changes. However, any flutter stability advantage gained by reprofiling must be weighed against bird strike worthiness requirements.

The underlying mechanism behind the changes in the flutter boundaries may be explained as follows. A section toward the tip of the fan blade at part speed typically operates with an expelled shock at a given back-pressure. As the LE becomes bluffer, the shock loss increases. Similarly, the profile loss increases due to the shock/boundary-layer interaction. This results in the blade achieving a lower pressure ratio and effectively operating on a degraded characteristic (Fig. 2a). To achieve the same back-pressure, the bluffer section compensates for the increased LE loss by operating further up its characteristic with a stronger and more expelled shock, increased angle of attack, and larger regions of separation. (Figure 4a shows lift distributions for each blade at 85% span for the same back-pressure.) The distribution of unsteady work done on the blade per cycle (Fig. 4b) at 85% span shows the shock is a stabilizing region on the suction surface, while the region behind the shock is destabilizing[7]; each region grows as back-pressure increases, with the destabilizing region becoming dominant. All four LE blades exhibit this type of behavior when the back-pressure is increased, but they experience zero aerodynamic damping at different pressure ratios and mass flow rates.

The level of aerodynamic damping determines the stability of the blade and is essentially a balance between the stabilizing and destabilizing regions of the blade; subtle changes in aerodynamics due to geometry will shift this balance. This suggests a complicated situation where the increased LE loss, associated with bluffness, reduces the aerodynamic damping or stability of the blade for a given back-pressure, that is, not only has the characteristic been reduced in pressure ratio, but the stability point has also moved substantially. This observed behavior is basically the "effect" of a reduction in aerodynamic damping, which has been "caused" by the increased parasitic loss associated with the deterioration of the aerodynamic LE shape.

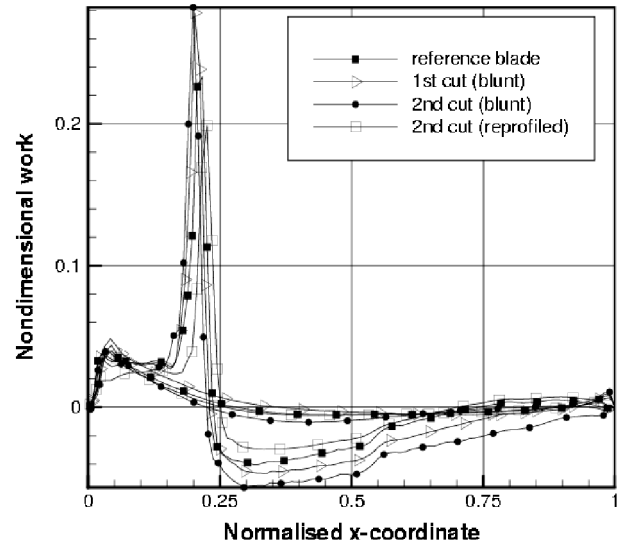

Fig. 4b Chordwise distribution of work done around the blade at the same back-pressure, 85% span (positive work stabilizing).

Conclusions

1) Steady flow computations on relatively coarse meshes are capable of capturing performance changes for different levels of bluffness of the LE profile. Future investigations should use finer meshes with attention being paid to the modeling of the LE.

2) The single-passage flutter calculations indicate that bluff-nosed LE profiles reduce flutter margins, as supported by the measured data.

3) Reprofiling the LE restores the flutter margin, with the chordal loss being of negligible significance. Although this would bias a design toward a more slender shape, other mechanical issues will ultimately limit this option.

Acknowledgments

The authors wish to thank Rolls–Royce, plc., for sponsoring some of the work presented in this Note and gratefully acknowledge many useful discussions with their colleagues at Rolls–Royce, plc., C. Freeman and J. G. Marshall.

References

[1]Suder, K. L., Chima, R. V., Strazisar, A. J., and Roberts, W. B., "The Effect of Adding Roughness and Thickness to a Transonic Axial Compressor Rotor," *Journal of Turbomachinery*, Vol. 117, No. 4, 1995, pp. 491–505.

[2]Sayma, A. I., Vahdati, M., Sbardella, L., and Imregun, M., "Modeling of Three-Dimensional Viscous Compressible Turbomachinery Flows Using Unstructured Hybrid Grids," *AIAA Journal*, Vol. 38, No. 6, 2000, pp. 945–954.

[3]Sayma, A. I., Vahdati, M., and Imregun, M., "Multi-Stage Whole-Annulus Forced Response Predictions Using an Integrated Non-Linear Analysis Technique—Part I: Numerical Model," *Journal of Fluids and Structures*, Vol. 14, No. 1, 2000, pp. 87–101.

[4]Sbardella, L., Sayma, A. I., and Imregun, M., "Semi-Structured Meshes for Axial Turbomachinery Blades," *International Journal for Numerical Methods in Fluids*, Vol. 32, No. 5, 2000, pp. 569–584.

[5]Vahdati, M., Bréard, C., Sayma, A. I., and Imregun, M., "Computational Study of Intake Duct Effects on Fan Flutter Stability," *AIAA Journal*, Vol. 40, No. 3, 2002, pp. 408–412.

[6]Vahdati, M., Sayma, A. I., and Imregun, M., "Multi-Stage Whole-Annulus Forced Response Predictions Using an Integrated Non-Linear Analysis Technique—Part II: Study of HP Turbine," *Journal of Fluids and Structures*, Vol. 14, No. 1, 2000, pp. 103–125.

[7]Vahdati, M., Sayma, A. I., Marshall, J. G., and Imregun, M., "Mechanisms and Prediction Methods for Fan Blade Stall Flutter," *Journal of Propulsion and Power*, Vol. 17, No. 5, 2001, pp. 1100–1108.

[8]Erdos, J. I., Alzner, E., and McNally, W., "Numerical Solution of Periodic Transonic Flow Through a Fan Stage," *AIAA Journal*, Vol. 15, No. 11, 1977, pp. 1559–1571.